IEEE Open Journal of
Antennas and Propagation

Received 27 September 2023; accepted 29 October 2023. Date of publication 7 November 2023; date of current version 1 December 2023.

Digital Object Identifier 10.1109/OJAP.2023.3330917

Accurate Determination of Antenna Gain in the 300-GHz Band Using Amplitude Center Estimated From Electrooptic Near-Field Measurements

YUTA HAYASHI, YU KATSUUE, YUSUKE TANAKA (Graduate Student Member, IEEE), AND SHINTARO HISATAKE (Member, IEEE)

Electrical and Energy System Engineering Division, Faculty of Engineering, Gifu University, Gifu 501-1193, Japan

CORRESPONDING AUTHOR: S. HISATAKE (e-mail: hisatake.shintaro.f4@f.gifu-u.ac.jp)

This work was supported by the National Institute of Information and Communications Technology (NICT), Japan, under Grant 19601 and Grant 04301.

ABSTRACT Antenna gain determination using the Friis equation typically employs the geometrically determined physical distance between antenna apertures, which often underestimates the gain. Herein, we propose and demonstrate an accurate antenna-gain determination method using the distance between the amplitude centers (ACs) of the antennas determined from the spatial phase distribution of the near field measured based on an electrooptic technique. Employing a WR-3.4 horn antenna, we show that at 286 GHz, the proposed method determines antenna gain with the same level of error even when the antenna separation distance is 1/5 shorter than that obtained using the conventional method that employs the physical distance between the antenna apertures in the Friis equation. Furthermore, the gain calculated using the proposed method achieves an error margin of <0.08 dB compared with that determined using the extrapolation method, which also utilizes the geometric physical distance between the antenna apertures. Notably, as the AC can be directly measured from the near-field distribution, the proposed method enables accurate antenna gain measurements without requiring prior knowledge of the characteristics and structural details of the antenna.

INDEX TERMS Amplitude center, antenna gain, EO measurement, far-field pattern, near-field measurement, phase center, terahertz.

I. INTRODUCTION

THE 300-GHZ band (220–330 GHz) is being considered to realize high-speed and high-capacity wireless communication in Beyond-5G/6G era scenarios, such as mobile applications and fixed point-to-point applications (e.g., intradevice communication, kiosk applications, and wireless backhaul/fronthaul) [1]. Because directivity increases with increasing frequency, accurately determining the antenna gain and the radiation pattern is crucial for such applications.

Currently, two standard methods are used for measuring antenna gain: the gain-comparison method (also known as the gain-transfer method) and the absolute-gain method [2]. The former requires a calibrated antenna or probe as a reference antenna and determines the gain by comparing the transmission characteristics of a reference antenna with those of the antenna under test (AUT). The absolute-gain method, on the other hand, does not require a reference antenna, and it allows the gain to be determined using an antenna of unknown gain. Both methods use the Friis equation for calculating the gain. However, the gain measurements wherein the distance between antenna apertures is $2D^2/\lambda$ (where D represents the maximum dimension of the radiator and λ represents the operating wavelength) lead to underestimates of the antenna gain on the order of 1 dB despite the fact that the far-field (FF) condition assumed in the Friis equation is satisfied [3], [4]. This underestimation occurs owing to the prevalent practice of considering the antenna aperture as a reference point for establishing the antenna separation distance in the measurements [5], [6]. In scenarios involving such physical reference points, the measurements must be performed at a minimum separation distance of $16\times2D^2/\lambda$ between the antenna apertures to restrict the gain reduction within 0.05 dB [4]. For a typical small horn antenna (20–25 dBi)

operating in the 300-GHz band, this distance would be several meters. For a 50-dBi 300-GHz-band antenna that is considered for wireless fronthaul/backhaul [7]—such as one with $D = 150$ mm—the distance would be 16×45 m $=$ 720 m, which is impractical for antenna testing. To reduce errors due to the short measurement distances used in gain measurements, gain-correction factors [4] and extrapolation methods [8] have been proposed, with the latter being widely adopted by various institutions for performing antenna gain measurements. The extrapolation method estimates the characteristics at infinity based on measurements conducted at multiple distances between antenna apertures. Although this method requires time-intensive measurements and the long-term stability of the measurement system, accurate gain determinations have been experimentally demonstrated for various antennas [8], [9].

An alternative approach is to determine the antenna gain using the distance between the electromagnetic reference points rather than the geometrically determined physical reference points. The amplitude center (AC) [10], from where the radiated field closely follows an inverse law, can be the electromagnetic reference point in the Friis equation [11]. Using the AC, which coincides with the average phase center (PhC) of the E- and H-planes [11], [12], as the antenna reference point, previous studies have demonstrated accurate antenna gain or antenna factor determinations. For instance, [13], [14] and, [15] have determined antenna gains using the PhC that is calculated through simulations. However, simulation-based methods are applicable only in limited situations where complete information about the AUT is available, and they are not applicable to unknown antennas, such as those enclosed in a radome. Reference [16] experimentally determined the PhC by repeatedly measuring the radiation patterns in the FF regime while adjusting the center of rotation of the transmitting antenna. However, repeated measurements of radiation patterns while moving the antenna rotation center are extremely complicated and time-consuming tasks, particularly when the approximate position of the PhC is not known.

In this paper, using the AC determined from the measured near-field (NF) distribution as the antenna reference point, we demonstrate that the antenna gain can be accurately determined in the 300-GHz band via short-range measurements. We demonstrate that the proposed approach can be applied even without a priori antenna knowledge. Schematic flow of the antenna gain determination along with the paper structure is illustrated in Figure 1. We conducted two distinct measurements, NF measurement and antenna gain measurement, using different experimental setups. In Section II-A, we measure the NF distribution at 286 GHz using an all-dielectric electrooptic (EO) probe featuring a small probe-head design, which facilitates low-disturbance and high-fidelity NF measurements [17], [18], [19]. In Section II-B, we determine the positions of the PhC numerically from the measured NF distribution. The position of AC is subsequently calculated by averaging the positions

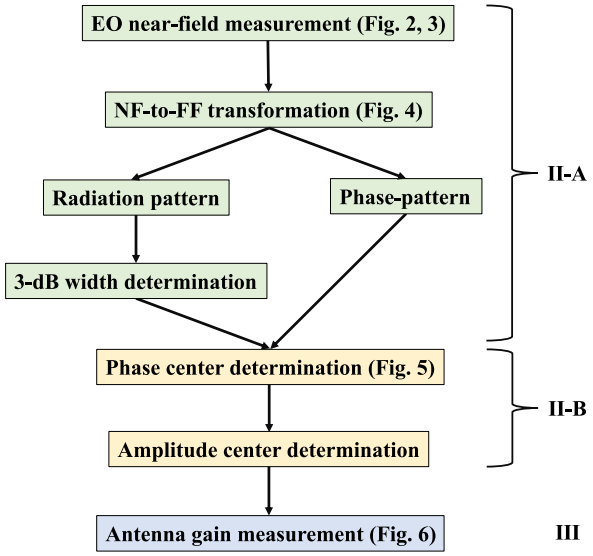

FIGURE 1. Schematic flow diagram of the antenna gain determination. The paper structure is also shown.

of the PhC of the E- and H-planes. In Section III, we confirm that the antenna gain obtained using the distance between ACs determined from the measured NF agrees to within 0.08 dB error with the gain determined using the conventional extrapolation method that employs the distance between antenna apertures at the frequency of the NF measurements. Conclusion is shown in Section IV.

II. DETERMINATION OF THE AC LOCATION

A. NF MEASUREMENTS

In this section, we describe measurements of the planar NF distribution of the AUT and determine the location of the AC from these measurements. The AUT we used was a WR-3.4 standard-gain horn antenna (RPG-Radiometer Physics GmbH, FH-SG-325-25). Figure 2 schematically depicts the setup for NF measurements. In this figure, the orange lines represent optical fibers, while the blue lines represent electrical cables or waveguides. We measured the electric field distribution using a self-heterodyne system [20] that is capable of acquiring both amplitude and phase information. This system uses optical beat notes generated by two free-running continuous waves (CWs) telecom lasers (193.4068 THz and 193.1212 THz), separated by approximately 286 GHz to generate and detect terahertz waves. We used a J-band uni-traveling-carrier photodiode (UTC-PD) to generate the signal and an EO probe comprising an organic EO crystal of DAST (4-N,N-Dimethylamino-4′-N′-methylstilbazolium tosylate) with dimensions of 0.5 mm $\times$ 0.5 mm $\times$ 0.3 mm mounted on a fiber for signal detection.

In the self-heterodyne system, the optical beat notes for the RF signal, which is supplied to the UTC-PD, and the local oscillator (LO) signal, which is supplied to the EO probe, have the same frequency/phase fluctuations though the different frequencies. Consequently, the frequency and phase fluctuations are canceled in the frequency downconversion process, enabling stable phase measurements. To attenuate

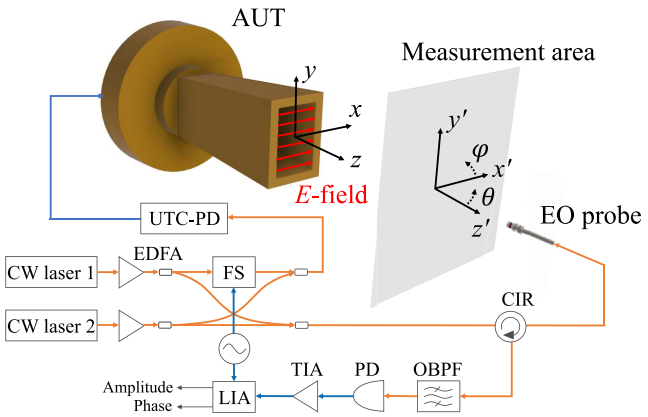

FIGURE 2. Schematic of the NF measurement setup and the FF coordinate system, where θ represents the polar angle and ϕ represents the azimuthal angle. When the NF distribution is transformed into the FF radiation pattern, the origin of the FF pattern is located at the center of the measurement plane. CW, continuous-wave; EDFA, erbium-doped fiber amplifier; FS, frequency shifter; UTC-PD, uni-traveling-carrier photodiode; AUT, antenna under test; CIR, circulator; EO, electrooptic; OBPF, optical band-pass filter; PD, photodiode; TIA, transimpedance amplifier; LIA, lock-in amplifier.

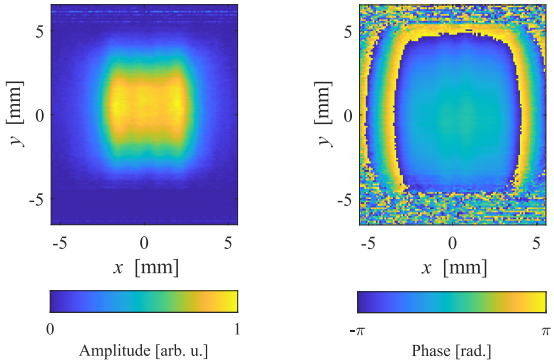

(a) Amplitude distribution (b) Phase distribution

FIGURE 3. (a) Normalized amplitude and (b) phase distributions of the NF electric field distribution E_x of the AUT measured using the EO probe. The presented images are averages of five measurements.

the impact of polarization fluctuations in optical fibers and EO crystals, we employed the nonpolarimetric frequency downconversion technique [21] that offers more stable phase measurements than the polarimetric techniques [22] employed in conventional EO sampling. In the nonpolarimetric technique, the probe light is phase modulated in the EO crystal using a continuous terahertz wave to generate modulation sidebands. Subsequently, the generated modulation sideband is mixed with the strong probe light (optical LO signal) for frequency downconversion [21]. The amplitude and phase information of the downconverted signals are detected using a lock-in amplifier and recorded during the planar scanning of the probe, facilitating the measurement of a two-dimensional amplitude and phase distribution of the electric field. The applicability of the self-heterodyne and nonplarimetric frequency downconversion techniques extends to a frequency range of 1–600 GHz [23], [24]. Therefore, these techniques are suitable for lower frequency bands such as millimeter-wave band and sub-6-GHz band.

The radiation pattern can be obtained by Fourier transforming the NF distribution [2]. The plane-wave spectrum $F_t(k_x, k_y)$ can be described as follows using the tangential component of the electric field E_t on the plane parallel to the antenna aperture:

$$F_t(k_x, k_y) = \int_{-L_y/2}^{+L_y/2} \int_{-L_x/2}^{+L_x/2} E_t(x, y, z = z_r) e^{j(k_x x + k_y y)} dx dy. \tag{1}$$

Here, k_x and k_y represent the spectral frequencies and L_x and L_y represent the dimensions of the measurement area in the x and y directions. z_r denotes the distance between the center of the antenna aperture and that of the measurement plane. For the coordinate system considered herein, x and y denote the tangential directions of the electric field. The radiation pattern $\mathbf{E}(r, \theta, \phi)$ of the antenna can then be obtained from

$$\mathbf{E}(r, \theta, \phi) \simeq j \frac{k_0 e^{-jk_0 r}}{2\pi r} \left[\cos\theta \mathbf{F}(k_x, k_y)\right] \tag{2}$$

using the plane-wave spectral function $\mathbf{F}(k_x, k_y)$, where k_0 represents the wavenumber defined as $2\pi/\lambda$. The measured NF distribution can be transformed into the radiation pattern using (2).

Figure 3 shows measurements of the amplitude and phase of the E_x component of the electric field at a frequency of 286 GHz [17]. The AUT was polarized in the x-direction, and measurements were performed with the sensitivity axis of the EO probe aligned with the x-axis. We positioned the probe 2 mm ($\approx 2\lambda$) from the antenna aperture in the z-direction and measured an area ($L_x \times L_y$) of 11 mm $\times$ 13 mm in 0.1 mm intervals to satisfy the Nyquist criteria. We averaged five measurements and normalized the amplitude using the maximum value within the measurement area. Considering that the size of the AUT aperture is 5.5 mm $\times$ 8.1 mm, the effective angular range [2] is approximately $\pm 50°$, as calculated from the geometric relation between the antenna aperture and measurement area.

Figure 4 shows the radiation pattern obtained by transforming the NF distribution along with the results obtained from simulations. In this study, we focus solely on the patterns in the E- and H-planes and examine only the phase pattern of the horizontal component. The simulations were conducted using a commercial full-wave electromagnetic simulator (CST Microwave Studio). In the simulations, the AUT was modeled as a perfect electrical conductor excited at 286 GHz via a waveguide port, with a maximum mesh cell size of $\lambda/10$. We assumed that the AUT will emit linearly polarized electromagnetic waves; the cross-polarization was neglected in the measurements, and (1) was evaluated using $F_y(k_x, k_y) = 0$. To comparatively analyze the phase patterns, the phase-reference point (origin of FF coordinates) was set in the simulation to be 2 mm in the z-direction from the center of the antenna aperture (Fig. 2). As for the measurements, we did not perform probe correction; the measured radiation patterns are raw

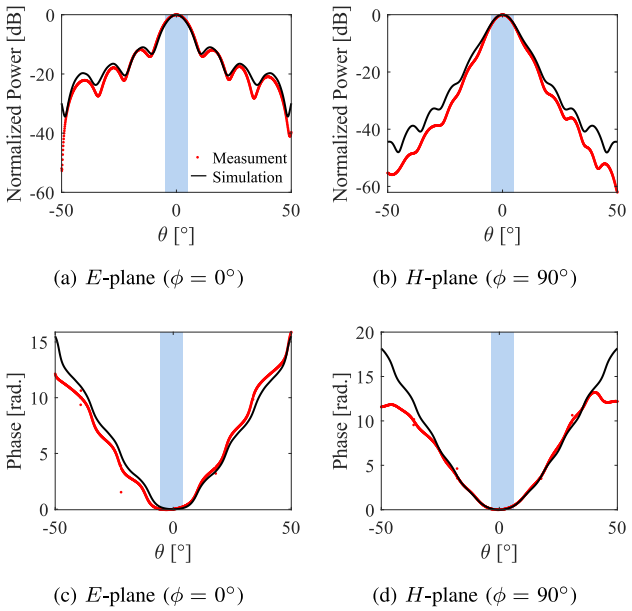

(a) E-plane ($\phi = 0°$) (b) H-plane ($\phi = 90°$)

(c) E-plane ($\phi = 0°$) (d) H-plane ($\phi = 90°$)

FIGURE 4. Normalized radiation patterns in (a) the *E*-plane and (b) the *H*-plane. The radiation patterns are shown with the maximum value aligned to 0°. The unwrapped phase patterns are shown in (c) the *E*-plane and (d) the *H*-plane. The red pattern represents the measured radiation pattern using a self-heterodyne system without probe correction, while the black pattern shows the simulation result. The patterns are shown only within the effective angular range.

data. Nevertheless, as shown in Fig. 4, the radiation patterns within the 3-dB beamwidth of the main lobe obtained from the measurements and simulation agree well. The maximum phase differences between the experiment and simulation within the 3-dB beamwidth were 0.22 rad for the E-plane and 0.04 rad for the H-plane. The slight discrepancy in the phase pattern within the 3-dB beamwidth of the E-plane can be attributed to alignment errors between the AUT and the scanning plane of the EO probe. However, as the angle θ increases, the observed discrepancy between the simulated radiation pattern and that calculated from the measured NF distribution increases. This is attributed to the angle-of-arrival-dependence characteristics of the EO probe used in the measurements [17]. Our technique can be applied to lower-gain antennas (having wider 3-dB beamwidth) by solving this issue based on probe correction [17] or replacing the planar scanning system with a cylindrical or spherical scanning system [25]. As discussed later, the PhC can be accurately determined from the phase data obtained within the 3-dB beamwidth of the main lobe—in this case ±4.8° from the direction of the main lobe [colored region in Figs. 4 (c) and (d)]. The process of determining PhC using the phase data within the 3-dB beamwidth is further elaborated in the subsequent Section II-B.

B. DETERMINATION OF THE PHC AND AC

The AC is equivalent to the average of the PhCs in the E- and H-planes [11], [12]. In this section, the PhCs in the E- and H-planes are determined from the measured phase distribution, and thereafter, the AC position is derived by averaging the PhC positions. The PhC is defined as the center of curvature of the phasefront in the FF region where radiation is significant [26]. According to this definition, the PhC is the reference point at which the phase pattern ideally becomes independent of the polar angle θ and the azimuthal angle ϕ in that portion of the wavefront where radiation is significant (i.e., within the 3-dB beamwidth).

In this study, to determine the distance of the PhC location relative to the center of the measurement plane, we analyzed the phase patterns of the FF pattern in the E-plane (θ-cuts with $\phi = 0°$; the xz-plane in Fig. 2) and the H-plane (θ-cuts with $\phi = 90°$; the yz-plane in Fig. 2). When the measured NF distribution is converted into the FF pattern using (1) and (2), the reference point of this phase pattern coincides with the center of the measurement plane ($z = z_r$). We denote this phase pattern as ψ. Furthermore, we denote the phase pattern as ψ' when the phase-reference point is moved from the center of the measurement plane by a displacement vector $\mathbf{r_d} = (x_d, y_d, z_d)$. The relation between ψ and ψ' can be written as ([27], [28]),

$$\psi_h'^{E}(\theta) = \psi_h^{E}(\theta) - k_0 \sin\theta x_d - k_0 \cos\theta z_d, \tag{3}$$

$$\psi_h'^{H}(\theta) = \psi_h^{H}(\theta) - k_0 \sin\theta y_d - k_0 \cos\theta z_d. \tag{4}$$

The superscripts E and H indicate the E-plane and H-plane patterns, respectively, and the subscript h indicates the horizontal component. Herein, we determine PhC location by finding the phase-reference point that minimizes the sum of the squared differences (SSD) between the FF phase pattern as a function of the angle θ and the constant value C (i.e., phase offset). In other words, we find the phase-reference point that minimizes the right-hand side of (5). This phase-reference point can be readily determined using the least-squares method, wherein the three variables—x_d, z_d and C for the E-plane and y_d, z_d, and C for the H-plane—are adjusted to obtain the minimal SSD [27], [29].

$$SSD = \sum_{i=1}^{N} \left(\psi_h'(\theta_i) - C\right)^2. \tag{5}$$

Here, i represents the i^{th} item of the phase pattern and N represents the total item number of the phase patterns.

We used the phase pattern within the average 3-dB beamwidth (±4.8° relative to the direction of the main lobe) to determine the PhC of the E- and H-planes. For the E-plane, the main-lobe direction is −0.6°, so we used the angular range $-5.4° \le \theta \le 4.2°$ of the phase pattern shown in Fig. 4(c) to evaluate (5). Likewise, for the H-plane, the main-lobe direction is 1.4°, hence, we used the angular range $-3.4° \le \theta \le 6.2°$ of the phase pattern shown in Fig. 4(d) to evaluate (5).

The minimum SSD is attained at $(x_{dE}, z_{dE}) = (0.3\text{ mm}, -6.1\text{ mm})$ for the E-plane and $(y_{dH}, z_{dH}) = (0.1\text{ mm}, -11.7\text{ mm})$ for the H-plane; these are the most suitable points for the PhCs. The values of x_{dE} and y_{dH} are nonzero because the aperture plane of the AUT is not strictly parallel to the measurement plane.

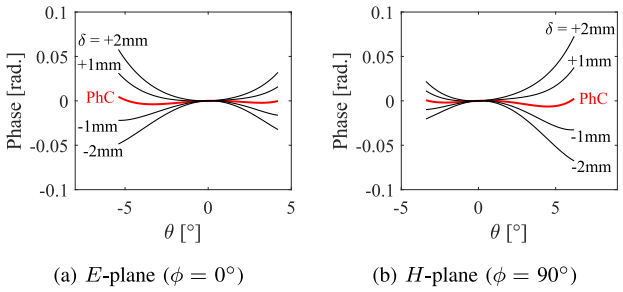

FIGURE 5. (a) *E*-plane and (b) *H*-plane phase patterns for different phase-reference points. The results are shown within a 3-dB beamwidth centered on the direction of the main lobe.

Figure 5 shows the variation of the phase patterns of $\psi_h^{'E}(\theta)$ and $\psi_h^{'H}(\theta)$ calculated using different phase-reference points. The red lines in Figs. 5(a) and (b) show the phase patterns calculated using the estimated PhCs as the phase-reference points, whereas the black lines are those calculated using the phase references points that deviate from the PhC by amounts δ in the z-direction. As evident from the figure, the phase patterns calculated using the estimated PhC—(x_{dE}, z_{dE}) for $\psi_h^{'E}(\theta)$ and (y_{dH}, z_{dH}) for $\psi_h^{'H}(\theta)$—are flatter than those calculated using the points that deviate by amounts δ, validating our procedure. These results confirm the validity of the PhC determined from the NF measurements. Notably, the accuracy of gain determination is governed by that of PhC position determination. Therefore, if the PhC of the AUT is not well-defined, the resulting gain error may be comparable with that obtained using the conventional method.

The distance from the center of the measurement plane to the average PhC of the E- and H-planes, i.e., the AC position [11], [12], can be written as $\sqrt{x_{dE}^2 + y_{dH}^2 + [(z_{dE} + z_{dH})/2]^2}$. The nonzero values of x_{dE} and y_{dH} are considered for the calculation. As the distance between the measurement plane and antenna aperture is $z_r = 2$ mm, the distance from the center of the antenna aperture to the AC can be estimated as $\Delta_{ac} = \sqrt{x_{dE}^2 + y_{dH}^2 + [(z_{dE} + z_{dH})/2]^2} - z_r = 6.9$ mm at 286 GHz. Moreover, we determined the AC of the AUT based on a simulation that uses the structure of the AUT and found that $\Delta_{ac} = 7.3$ mm, which is in close agreement with the previous estimate, differing by only 0.4 mm.

For the sake of simplicity, we employed linearly polarized antennas with a known polarization state (x-polarization). If the antenna polarization is unknown, measuring the electric field distribution for both x- and y-polarizations is essential. To determine the AC for y-polarization, the probe must be rotated by 90° to obtain the electric field distribution E_y; the PhC can then be determined using the vertical component of the electric field E_v in our coordinate system.

III. ANTENNA GAIN MEASUREMENTS

A. MEASUREMENT SETUP

In this section, we compare the results of gain measurements obtained using the distance between the ACs (d_c) with the results obtained using the conventional extrapolation method that employs the distance (d_a) between the antenna apertures. The gain measurements are based on the two-antenna method [2] with a vector network analyzer (VNA; Keysight, N5242A). Figure 6(a) shows the setup for the gain measurements, and Figure 6(b) shows the relation between the distance d_a and the distance d_c. The photograph shown in 6(a) was captured during the positioning process, and the antennas were in contact with each other ($d_a = 0$). The quantity Δ_t represents the distance from the center of the antenna aperture to the AC of the transmitting antenna, and Δ_r represents the corresponding quantity for the receiving antenna. Herein, we used identical transmitting and receiving antennas; therefore, $\Delta_t = \Delta_r = \Delta_{ac} = 6.9$ mm.

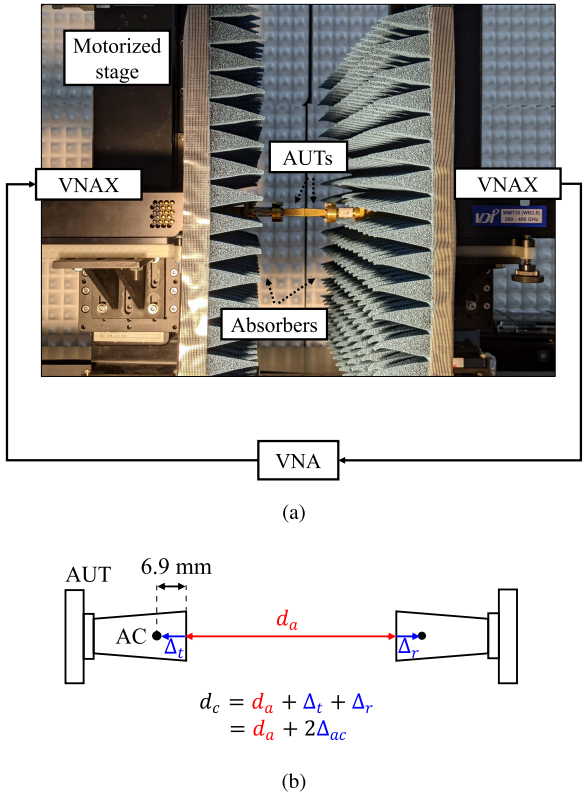

FIGURE 6. (a) Photograph of the antenna gain measurement setup. (b) Schematic diagram of the relation between d_a and d_c. Because identical AUTs are used in antenna gain measurement, $\Delta_t = \Delta_r = \Delta_{ac}$. The photograph shown in (a) was captured during the positioning process, and the antennas were in contact with each other.

The transmitting and receiving antennas used herein were the WR-3.4 standard-gain horn antennas discussed in Section II. We positioned the antennas facing each other. We connected a VNA extender (VNAX; Virginia Diodes Inc., WR-2.8VNAX), equipped with a WR-2.8 to WR-3.4 tapered waveguide, to the VNA to measure the forward-transmission coefficient $|S_{21}|^2$. Further, the system was calibrated via short-offset-short-load-through calibration, with the tip of the tapered waveguide used as the reference plane. This eliminated the influence of the transmission characteristics of the cable, VNAX, and tapered waveguide.

We performed the measurements in an anechoic chamber, with terahertz absorbers surrounding the measurement setup

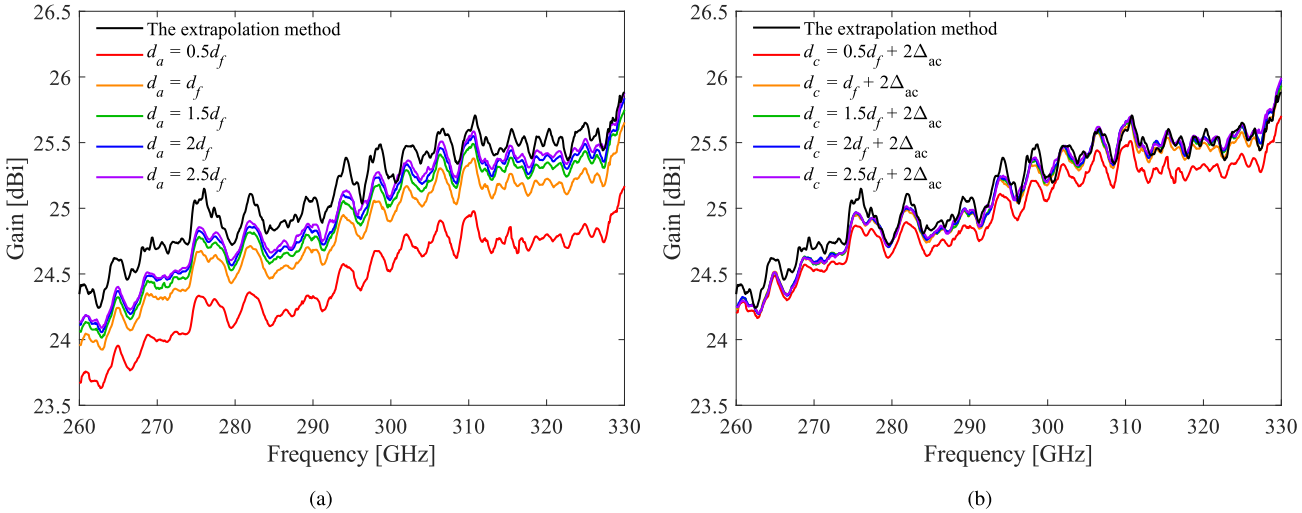

FIGURE 7. Frequency characteristics of the antenna gain measured at each antenna separation distance. We used (a) the distance d_a and (b) the distance d_c in (7). The results of gain measurements obtained using the extrapolation method (black line) are also shown for comparison.

to reduce unnecessary reflections. The frequency range of the VNA was set to 260–330 GHz (the overlapping band of WR-2.8 and WR-3.4), with a frequency interval of 0.1 GHz and an intermediate-frequency bandwidth of 1 kHz.

B. GAIN DETERMINATION USING THE AC

The antenna gain is calculated from the Friis equation, which can be written as follows:

$$|S_{21}|^2 = \frac{P_r}{P_t} = G_t G_r \left(\frac{\lambda}{4\pi d}\right)^2, \tag{6}$$

where G_t and G_r denote the gains of the transmitting and receiving antennas, respectively, λ indicates the operating wavelength, and d represents the distance between antennas. If the polarization correspondence is ideal, the resulting value of $|S_{21}|^2$ corresponds to the transmitting and receiving power ratio P_r/P_t (P_t = transmitted power and P_r = received power), as expressed in (6). Assuming that the two antennas are identical ($G = G_t = G_r$), (6) can be expressed in the decibel form as

$$G^{dBi} = \frac{1}{2}\left(S_{21}^{dB} + 20\log\frac{4\pi d}{\lambda}\right). \tag{7}$$

Conventionally, the distance between antenna apertures [d_a in Fig. 6(b)] is used as d in (7). Herein, we use instead the distance between ACs [d_c in Fig. 6(b)] as the distance d in (7).

In principle, the antenna gain can be determined from the data measured at a single distance. However, to reduce the influence of standing waves due to multiple reflections between antennas, we conducted $|S_{21}|^2$ measurements while varying the distance between the antennas at $\lambda/10$ intervals over one wavelength. The gain for each distance ($\lambda/10$ interval) was calculated using (7), and the results obtained at each distance were averaged; ten $|S_{21}|^2$ measurements were performed and averaged for each distance to improve the signal-to-noise ratio.

C. GAIN DETERMINATION BASED ON THE EXTRAPOLATION METHOD

The extrapolation method is a technique for calculating antenna gain by measuring the transmission characteristics while varying the distance between antenna apertures and fitting the measured $|S_{21}|^2$ to the expression

$$|S_{21}(d_a)\cdot d_a|^2 = A_0 + \frac{A_1}{d_a} + \frac{A_2}{d_a^2} + \cdots + \frac{A_n}{d_a^n} + \ldots, \tag{8}$$

where A_n denotes the polynomial coefficient of the n^{th}-order term. The extrapolation method recommends measuring the transmission characteristics at 100–1000 points at distances in the range $0.1d_f$–d_f [8]. Herein, we presumed the FF distance to be $d_f = 2D^2/\lambda_{min} \simeq 211$ mm based on the shortest wavelength in the measured frequency band, λ_{min} = 0.9 mm (330 GHz), and D = 9.8 mm. We measured the $|S_{21}|^2$ at 201 points while varying the distance d_a from 10 to 220 mm. We varied the distance d_a such that the reciprocals of d_a were uniformly spaced. We measured $|S_{21}|^2$ five times at each point, computed the average, and fitted the obtained values of $|S_{21}|^2$ to a third-order polynomial. We then estimated the value A_0 of $|S_{21}\cdot d_a|^2$ at infinity from the intercept of the regression curve. Further, we determined the antenna gain from the following equation:

$$G^{dBi} = \frac{1}{2}\left(A_0^{dB} + 20\log\frac{4\pi}{\lambda}\right). \tag{9}$$

D. RESULTS AND DISCUSSION

Figures 7(a) and (b) show the measurements of antenna gain when the distances d_a and $d_c = d_a + 2\Delta_{ac}$ were used in (7), respectively. We measured data at the distances $d_a = 0.5d_f$, d_f, $1.5d_f$, $2d_f$, and $2.5d_f$. The ripples observed in Figure 7 can be attributed to the undesired multiple reflections that occurred in the measurement system including at WR-2.8-to-WR-3.4 transition, absorbers, etc. Figures 7 (a) and (b) also include measurements of the antenna gain obtained

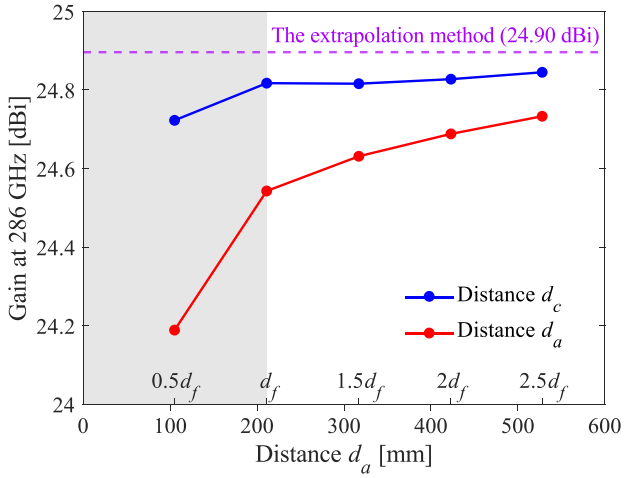

FIGURE 8. Antenna gains determined at each antenna separation distance. The blue points show the gains obtained using $d_c = d_a + 2\Delta_{ac}$ and the red points show the corresponding results obtained using d_a in (7) at 286GHz. The gray background represents the NF region ($< d_f$).

using the extrapolation method as the reference. All data shown in Figure 7 were obtained by applying moving-average at 1-GHz intervals. Using the distance d_a in (7), the measured gain results agree better with the result of the extrapolation method as the distance d_a increases, as shown in Fig. 7 (a). However, when using the distance d_c in (7), the overall results of gain measurements were in good agreement with the result of the extrapolation method, regardless of the distance d_c. Notably, computing the AC over multiple frequencies instead of determining it over a single frequency (in this case at 286 GHz) facilitates a more rigorous calibration, thereby further enhancing the gain measurement accuracy.

Figure 8 shows the antenna gain measured at 286 GHz as the distance d_a between antenna apertures was changed from 0.5 d_f to 2.5 d_f. The antenna gain at $d_a = 0.5d_f$—calculated using the distance d_a in (7)—underestimated the gain determined using the extrapolation method by more than 0.7 dB. As the distance d_a increased, the discrepancy decreased. The discrepancy was 0.16 dB at $d_a = 2.5d_f$. Conversely, when we used the distance d_c in (7), the deviation from the result of the extrapolation method was 0.17 dB even at the 1/5 shorter distance of $d_a = 0.5d_f$. The deviation from the results of the extrapolation method was 0.08 dB at $d_a = d_f$, which is the FF distance of the AUT. In case of $d_a = 0.5d_f$ (in the NF region), the gain is underestimated because (7) is valid for the FF region.

IV. CONCLUSION

We demonstrated that antenna gain can be accurately determined in the 300-GHz band using the AC—which we determined from the NF distribution measured using an EO sensing technique—as the antenna reference point in the Friis equation. Because the AC can be determined through direct measurements of the NF distribution, this method has the feature that accurate antenna gain measurements can be performed without prior knowledge of the antenna.

We employed a WR-3.4 horn antenna as the AUT and demonstrated that at 286 GHz, the position of the AC determined from the NF measurements agreed well with the simulation results, i.e., to within an error of 0.4 mm. We confirmed that the antenna gain determined from the two-antenna method, using the distance between ACs in the Friis equation, agreed well with the gain determined using the extrapolation method that employs the distance between antenna apertures; i.e., to within an error less than 0.08 dB. Moreover, we confirmed that using the distance between ACs in the Friis equation determines gain with the same level of error even when the antenna separation distance is 1/5 shorter than that obtained using the conventional method that employs the distance between the antenna apertures in the Friis equation.

Therefore, the proposed approach can more accurately and time-efficiently determine the antenna gain for compact gain-measurement systems that will be applied in the Beyond-5G/6G era, where the FF distances increase with increasing frequencies.

REFERENCES

[1] T. Kürner, "THz communications—A candidate for a 6G radio?" in *Proc. 22nd Int. Symp. Wireless Pers. Multimedia Commun. (WPMC)*, 2020, pp. 1–5. [Online]. Available: https://leopard.tu-braunschweig.de/receive/dbbs_mods_00068882
[2] C. A. Balanis, *Antenna Theory: Analysis and Design*, 2nd ed. New York, NY, USA: Wiley, 1997, pp. 852–858.
[3] E. H. Braun, "Gain of electromagnetic horns," *Proc. IRE*, vol. 41, no. 1, pp. 109–115, 1953.
[4] T. S. Chu and R. A. Semplak, "Gain of electromagnetic horns," *Bell Syst. Tech. J.*, vol. 44, no. 3, pp. 527–537, Mar. 1965.
[5] M. Alibakhshikenari et al., "High gain/bandwidth off-chip antenna loaded with metamaterial unit-cell impedance matching circuit for sub-terahertz near-field electronic systems," *Sci. Rep.*, vol. 12, no. 1, 2022, Art. no. 17893.
[6] K. Fujii, T. Tosaka, Y. Matsumoto, and A. Kasamatsu, "Calibration of standard gain horn antennas in the frequency range from 220 to 325 GHz," in *Proc. 38th Int. Conf. Infrared Millimeter Terahertz Waves (IRMMW-THz)*, 2013, pp. 1–2.
[7] Z.-K. Weng et al., "Millimeter-wave and terahertz fixed wireless link budget evaluation for extreme weather conditions," *IEEE Access*, vol. 9, pp. 163476–163491, 2021.
[8] A. Newell, R. Baird, and P. Wacker, "Accurate measurement of antenna gain and polarization at reduced distances by an extrapolation technique," *IEEE Trans. Antennas Propag.*, vol. 21, no. 4, pp. 418–431, Jul. 1973.
[9] A. Repjar, A. Newell, and D. Tamura, "Extrapolation range measurements for determining antenna gain and polarization," U.S. Dept. Commer., Nat. Bureau Stand., Washington, DC, USA, 1987.
[10] J. Appel-Hansen, "Centers of structures in electromagnetism—A critical analysis," *IEEE Trans. Antennas Propag.*, vol. 30, no. 4, pp. 606–610, Jul. 1982.
[11] A. Panicali and M. Nakamura, "On the amplitude center of radiating apertures," *IEEE Trans. Antennas Propag.*, vol. 33, no. 3, pp. 330–335, Mar. 1985.
[12] M. Hirose, M. Ameya, and S. Kurokawa, "Relation between phase center and amplitude center of antenna by Kern transmission formula," in *Proc. Int. Symp. Antennas Propag. (ISAP)*, 2012, pp. 1015–1018.
[13] K. Harima, "Evaluating the effectiveness of applying the phase center for antenna measurements," in *Proc. IEEE Conf. Antenna Meas. Appl. (CAMA)*, 2017, pp. 61–64.
[14] K. Harima, "Numerical simulation of far-field gain determination at reduced distances using phase center," *IEICE Trans. Commun.*, vol. E97.B, no. 10, pp. 2001–2010, 2014.

[15] Z. Chen, M. Foegelle, and T. Harrington, "Analysis of log periodic dipole array antennas for site validation and radiated emissions testing," in *Proc. IEEE Int. Symp. Electromagn. Compatabil. Symp. Rec.*, vol. 2, 1999, pp. 618–623.

[16] Y. Tamaki, T. Kobayashi, and A. Tomiki, "Precise determination of phase centers and its application to gain measurement of spacecraft-borne antennas in an anechoic chamber," in *Proc. 38th Annu. Meeting Symp. Antenna Meas. Techn. Assoc. (AMTA)*, 2016, pp. 14–20.

[17] Y. Tanaka et al., "Photonics-based near-field measurement and far-field characterization for 300-GHz band antenna testing," *IEEE Trans. Antennas Propag.*, vol. 3, pp. 24–31, 2022.

[18] S. Hisatake, H. H. Nguyen Pham, and T. Nagatsuma, "Visualization of the spatial–temporal evolution of continuous electromagnetic waves in the terahertz range based on photonics technology," *Optica*, vol. 1, no. 6, pp. 365–371, Dec. 2014. [Online]. Available: https://opg.optica.org/optica/abstract.cfm?URI=optica-1-6-365

[19] S. Hisatake et al., "Mapping of electromagnetic waves generated by free-running self-oscillating devices," *Sci. Rep.*, vol. 7, no. 1, p. 9203, Aug. 2017. [Online]. Available: https://doi.org/10.1038/s41598-017-09802-0

[20] S. Hisatake, G. Kitahara, K. Ajito, Y. Fukada, N. Yoshimoto, and T. Nagatsuma, "Phase-sensitive terahertz self-heterodyne system based on photodiode and low-temperature-grown gaas photoconductor at 1.55 μm," *IEEE Sensors J.*, vol. 13, no. 1, pp. 31–36, Jan. 2013.

[21] S. Hisatake and T. Nagatsuma, "Nonpolarimetric technique for homodyne-type electrooptic field detection," *Appl. Phys. Exp.*, vol. 5, no. 1, Dec. 2011, Art. no. 12701. [Online]. Available: https://dx.doi.org/10.1143/APEX.5.012701

[22] H. Togo, A. Sasaki, A. Hirata, and T. Nagatsuma, "Characterization of millimeter-wave antenna using photonic measurement techniques," *Int. J. RF Microw. Comput.-Aided Eng.*, vol. 14, no. 3, pp. 290–297, 2004. [Online]. Available: https://onlinelibrary.wiley.com/doi/abs/10.1002/mmce.20012

[23] H. Takeuchi and S. Hisatake, "Microwave signal detection based on the nonpolarimetric frequency down-conversion technique," *IEEE Sensors Lett.*, vol. 4, no. 9, Sep. 2020, Art. no. 3501204.

[24] S. Hisatake, *Millimeter-Wave and THz-Wave Visualization*. Singapore: Springer, 2023, pp. 1–34. [Online]. Available: https://doi.org/10.1007/978-981-33-4999-5_31-1

[25] Y. Tanaka and S. Hisatake, "Cylindrical near-field measurement and far-field characterization of 300-GHz band antenna based on an electrooptic measurement technique," in *Proc. Antenna Meas. Techn. Assoc. Symp. (AMTA)*, 2022, pp. 1–4.

[26] *IEEE Standard Definitions of Terms For Antennas*, IEEE Standard 145–1983, 1983, pp. 1–31.

[27] P. N. Betjes, "An algorithm for automated phase center determination and its implementation," in *Proc. 29th Annu. Symp. Antenna Meas. Techn. Assoc.*, 2007, pp. 1–6.

[28] J.-P. Shang, D.-M. Fu, Y.-B. Deng, and S. Jiang, "Measurement of phase center for antenna with the method of moving reference point," in *Proc. 8th Int. Symp. Antennas Propag. EM Theory*, 2008, pp. 114–117.

[29] D. Ma, S. G. Yang, Y. Q. Wang, W. R. Huang, and L. Hou, "A novel method for antenna phase center calibration," in *Proc. Int. Symp. Antennas Propag.*, vol. 1, 2013, pp. 259–261.